Energetic particle dynamics in Mercury's magnetosphere

B. M. Walsh,[1] A. S. Ryou,[1,2] D. G. Sibeck,[1] and I. I. Alexeev[3]

Received 17 October 2012; revised 26 February 2013; accepted 4 April 2013; published 13 May 2013.

[1] We investigate the drift paths of energetic particles in Mercury's magnetosphere by tracing their motion through a model magnetic field. Test particle simulations solving the full Lorentz force show a quasi-trapped energetic particle population that gradient and curvature drift around the planet via "Shabansky" orbits, passing though high latitudes in the compressed dayside by equatorial latitudes on the nightside. Due to their large gyroradii, energetic H^+ and Na^+ ions will typically collide with the planet or the magnetopause and will not be able to complete a full drift orbit. These simulations provide direct comparison for recent spacecraft measurements from *MESSENGER*. Mercury's offset dipole results in an asymmetric loss cone and therefore an asymmetry in particle precipitation with more particles precipitating in the southern hemisphere. Since the planet lacks an atmosphere, precipitating particles will collide directly with the surface of the planet. The incident charged particles can kick up neutrals from the surface and have implications for the formation of the exosphere and weathering of the surface.

Citation: Walsh, B. M., A. S. Ryou, D. G. Sibeck, and I. I. Alexeev (2013), Energetic particle dynamics in Mercury's magnetosphere, *J. Geophys. Res. Space Physics*, *118*, 1992–1999, doi:10.1002/jgra.50266.

1. Introduction

[2] The Mariner 10 flybys of Mercury in 1974 identified a global internal magnetic field [*Ness et al.*, 1974]. This lead to a discussion of whether trapped charged particles could exist within Mercury's magnetosphere. Through flybys by *MESSENGER* in 2008 and 2009 and observations after orbital insertion in 2011, the internal magnetospheric environment has become better understood. The internal magnetic field is well represented by an offset dipole centered on the spin axis [*Anderson et al.*, 2011, 2012]. The dipole is offset by 484 km (0.16 R_M) to the north geographic equator. A dipole tilt angle of $0° \pm 3°$ relative to the planet's rotational axis was also determined. Within the magnetosphere, thermal populations of electrons and protons as well as heavy ion species have been identified [*Zurbuchen et al.*, 2008].

[3] The first identification of energetic particles in Mercury's magnetosphere came from Mariner 10 which measured high-energy electrons ($E > 174$ keV) on the nightside of the planet. Several studies attribute these bursts to sequential substorms [*Christon et al.*, 1979; *Eraker and Simpson*, 1986]. The sequence of substorms cause a series of flux enhancements each lasting 5–10 s. In contrast, *Baker et al.* [1986] suggested that there could be a single substorm particle injection. The particles' gradient and curvature drift around the planet where they are repeatedly observed on the nightside. This is analogous to drift echoes observed within the Earth's radiation belts [*Belian et al.*, 1984]. This explanation relies on electrons being magnetically trapped in Mercury's magnetosphere.

[4] The existence of a trapped charged particle population analogous to that in the Earth's radiation belt has been debated since the discovery of Mercury's magnetic field [*Ip*, 1987]. Since Mercury's magnetosphere is roughly a factor of 8 smaller than the Earth's, scaling the Earth's radiation belts at 4–5 R_E to Mercury would bring the trapped population to <1 R_M. Despite this, there have been a number of numerical simulations showing that particles could be magnetically trapped in Mercury's magnetosphere. These simulations include test particle modeling of sodium [*Yagi et al.*, 2010] as well as hybrid simulations of 1–10 keV ions and electrons [*Schriver et al.*, 2011], both indicating the existence of a quasi-trapped population. The populations generally occur from radial distances of ~1.3 R_M to 1.5 R_M [*Trávníček et al.*, 2007, 2009]. The term "quasi-trapped" here means a population that can be magnetically trapped for several orbits around the planet but not necessarily for weeks and months as in the Earth's magnetosphere.

[5] The current work looks at suprathermal particles and their dynamics within Mercury's magnetosphere under northward interplanetary magnetic field (IMF). The Lorentz force is solved to trace the particle motion in a realistic magnetic field model. First, the paths of individual particles are studied in section 4, then an ensemble of particles is studied in section 4.1. Modeling shows a quasi-trapped electron population as well as significant amounts of charged particles precipitating to the surface of the planet.

[1]NASA Goddard Space Flight Center, Greenbelt, Maryland, USA.
[2]Department of Physics, University of Chicago, Chicago, Illinois, USA.
[3]Scobeltsyn Institute of Nuclear Physics, Lomonosov Moscow State University, Moscow, Russia.

Corresponding author: B. M. Walsh, NASA Goddard Space Flight Center, Greenbelt, MD, USA. (brian.m.walsh-1@nasa.gov)

2169-9380/13/10.1002/jgra.50266

2. Particle Trajectories

[6] In a highly compressed dipole magnetic field, similar to Mercury's magnetosphere, there is no magnetic minimum near the dayside equator, but there are two magnetic minima at off-equatorial latitudes on the dayside. Energetic particles drifting along contours of constant magnetic field strength through the equatorial nightside magnetosphere can transit the dayside magnetosphere by moving to high latitudes. This bifurcation of the drift shell is often called a "Shabansky" orbit [*Shabansky*, 1971]. The initial pitch angle of the particle is also important as the magnetic maximum at the equator on the compressed dayside must be large enough to mirror the particle. A particle population with initial pitch angle close to 90° will bifurcate under a smaller compression than a field-aligned particle. The motion of outer radiation belt populations along such bifurcating drift paths on Earth has been analyzed in a number of studies [*Öztürk and Wolf*, 2007; *Wan et al.*, 2010; *Ukhorskiy et al.*, 2011]. As particles travel to high latitude, the bounce path changes and the second adiabatic invariant is broken. On Mercury, the magnetic geometry is so compressed that a large fraction of the quasi-trapped population must exhibit this orbit.

[7] Figure 1 shows contours of magnetic field strength in the equatorial plane from the *Alexeev et al.* [2008, 2010] model. The blue region is where the minimum magnetic field strength lies off the equator. This region is identified by calculating the second derivative of the magnetic field strength along a field line $\left(\frac{d^2B}{ds^2}\right)$. If $\frac{d^2B}{ds^2} < 0$, then the particle drift paths will start to bifurcate. This condition means particles with appropriate pitch angles can begin to mirror at the equatorial magnetic maximum. In the Earth's magnetosphere, the region where $\frac{d^2B}{ds^2} < 0$ is found only extends a few R_E from the magnetopause or a fraction of the distance from the subsolar magnetopause. In Mercury's magnetosphere, this region fills a large portion of Mercury's inner magnetosphere and all of the closed field lines on the dayside. While passing through this region of bifurcation, particles do not conserve their second adiabatic invariant. To further study the changes to a particle's second invariant, *Öztürk and Wolf* [2007] provides a theoretical expression which can be applied to different magnetic field models.

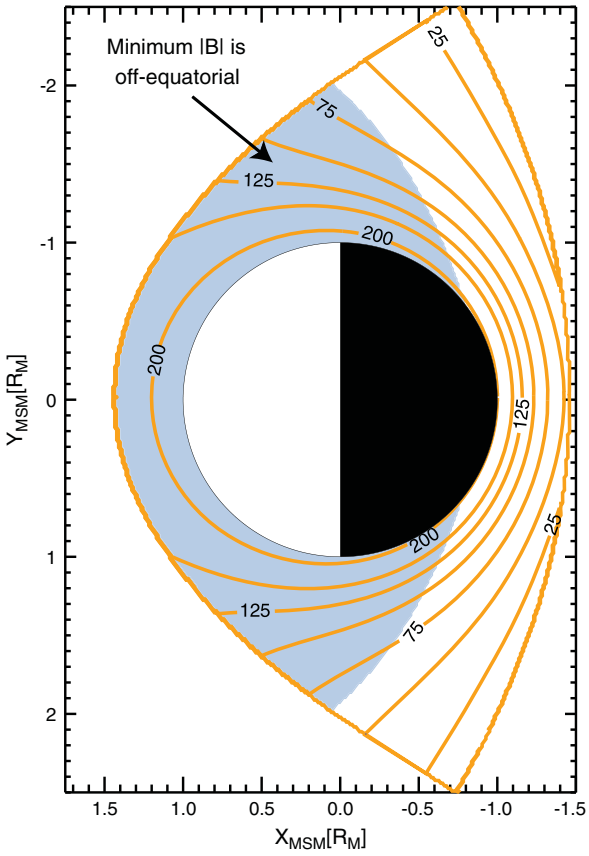

Figure 1. Contours of constant magnetic field strength in the equatorial plane from the *Alexeev et al.* [2008] model are shown in orange. The labels are in nanotesla. The blue region is where the magnetic minimum is off the equator. Depending on pitch angle, particles will begin to bifurcate to the north or south in this region.

3. Modeling

[8] Previous studies have shown nonadiabatic effects to be very important for heavy ions as well as energetic particles within Mercury's magnetosphere [*Delcourt et al.*, 2002, 2003]. To capture the dynamics of these particles, the full equation of motion is needed. In the current study, we integrate the motion of charged particles in Mercury's magnetosphere with the equation of motion given by equation (1):

$$m\frac{d(\gamma\vec{u})}{dt} = q\left[\vec{E} + \vec{u}\times\vec{B}\right] + m\vec{g} \quad (1)$$

[9] Equation (1) is solved with a sixth-order Runge-Kutta method. The mass, charge, and velocity are given by the variables m, q, and $\vec{u}$, respectively. The term $\vec{g}$ is gravitational acceleration or $(GM_M/r^2)\,\hat{r}$. The step size used is 1% of the gyrofrequency. Magnetic field values (B) are obtained from the *Alexeev et al.* [2008, 2010] model with a dipole offset of 484 km north of the geographic equator, no dipole tilt, and a planetary moment of 195 nT/R_M^3. The Alexeev paraboloidal magnetic field model incorporates an internal magnetic field, magnetopause current, and tail current sheet. A magnetopause flaring parameter of 0.5 and standoff distance of 1.45 R_M as has been found through studies from *MESSENGER* [*Johnson*, 2012] are used as inputs for the current study.

[10] For southward IMF, when dayside reconnection is active, a dawn-dusk electric field on Mercury has been determined by *Slavin et al.* [2009] through estimates of the motional solar wind electric field. With measurements of solar wind velocity and magnetic field and estimating an X-line length of 3 R_M, *Slavin et al.* [2009] calculated a cross polar cap potential of 30 kV which corresponds to a dawn-dusk electric field of ~2 mV/m. During northward IMF, reconnection is expected to be far less significant. This study models the magnetosphere in a steady state with $\vec{B}_{IMF}$ = (0, 0, 30) nT input to the magnetic field model. Since a northward IMF is used, the cross polar cap potential will be low and the dawn-dusk electric field is taken as $\vec{E}$ = 0 mV/m. During times of southward IMF when the electric field is anticipated to be larger in magnitude, the influence of the

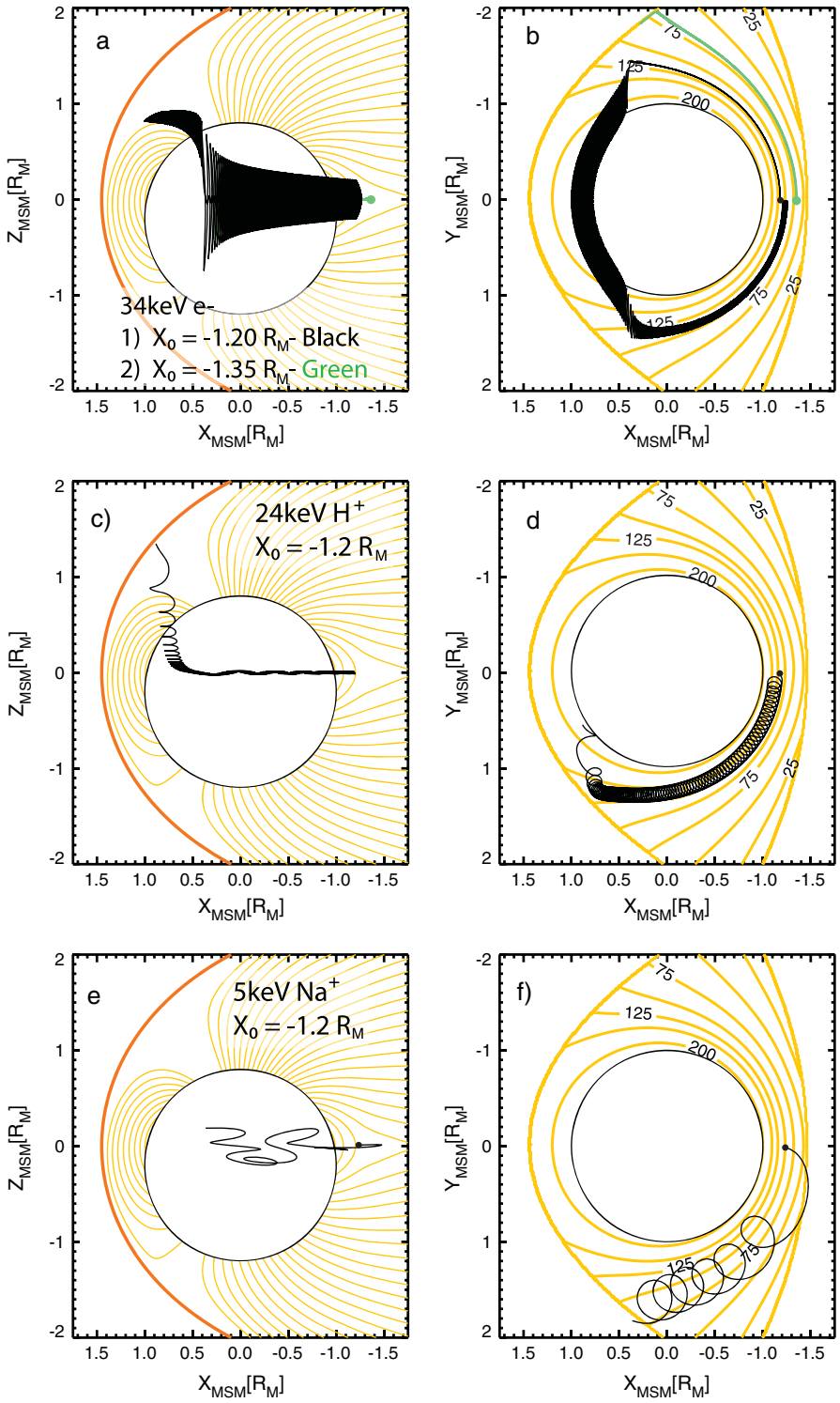

Figure 2. Single particle drifts of (a and b) electrons, (c and d) H^+, and (e and f) Na^+ ions. The left column are *XZ* cuts of particle traces and magnetic field lines. The right column are *XY* cuts with particle traces and magnetic field strength contours in the equatorial plane. Labels are in units of nanotesla.

electric field on the particle's trajectory is greater than the impact of gravity. The coordinate system used to describe the IMF vector throughout this study is Mercury solar magnetospheric (MSM). This is analogous to the geocentric solar magnetic (GSM) coordinate system on Earth. The positive *X* axis is directed from the center of the planet toward the sun; the *Y* axis is perpendicular to the *X* axis and points from the dawn to dusk along the terminator; and the *Z* axis points in the direction of the magnetic pole, but is shifted northward of the geographic equator by 484 km.

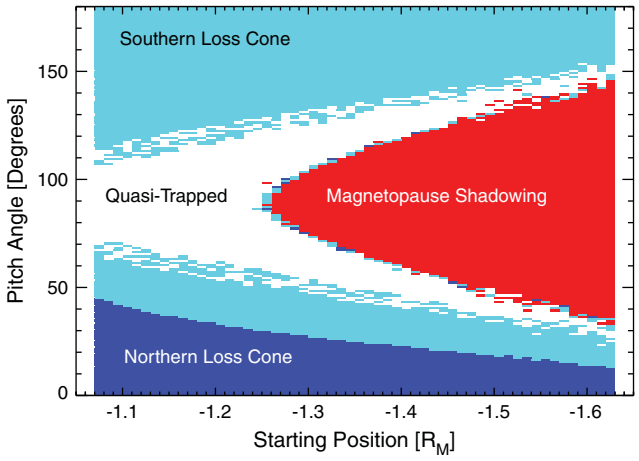

Figure 3. Initial start position in the X axis and pitch angle of 34 keV test electrons are given on the X and Y axes. All particles are started with $Z_{MSM} = Y_{MSM} = 0\,R_M$. Color indicates the final result of the particle. Light blue means the particle collided with the southern hemisphere, dark blue means the particle collided with the northern hemisphere, red means the particle is lost due to magnetopause shadowing, and white means the particle is trapped for at least 80 s (∼1.3 drift periods).

[11] Mercury's magnetosphere however has been observed to be quite dynamic [*Slavin et al.*, 2009, 2010; *Sundberg et al.*, 2012]; therefore, assuming a steady magnetosphere is not appropriate for long periods. The drift period of a 34 keV electron is roughly 64 s, which means the upstream solar wind conditions only need to be steady for ∼2–3 min for several drifts to be completed. Periods of steady northward IMF for several minutes are relatively common, so the assumption of a steady state magnetosphere is reasonable for these time scales.

4. Results

[12] Tracing of energetic electrons in Mercury's magnetosphere shows that charged particles can be magnetically trapped for at least several drift periods. This study first analyzes the dynamics of individual particles then looks at a larger population. Figures 2a and 2b show the drift paths of two 34 keV electrons. An electron with an initial pitch angle of 90° and starting beyond $X \sim -1.25\,R_M$ will simply drift into the dawn magnetopause and be lost from the magnetosphere (green trace). An electron with an initial pitch angle of 90° and starting inside of approximately –1.25 R_M will drift along a bifurcating drift shell (black trace) and remain within the magnetosphere. Thirty-four keV is selected since it is the lower energy threshold of the energetic electron sensor [*Andrews et al.*, 2007] on the *MESSENGER* spacecraft and can be used to compare with observations.

[13] A 24 keV H^+ ion has a larger gyroradius (228 km or 0.1 R_M) than the electron and cannot complete a full orbit (Figures 2c and 2d). The particle starts at $X = -1.2\,R_M$, $Y = Z = 0.0\,R_M$, drifts to the dayside, and attempts to go to high latitude but collides with the dusk magnetopause. When a particle collides with the magnetopause, it is assumed to be lost from the magnetosphere. Since the typical standoff position of the magnetopause is 1.45 R_M, and the particle attempts to follow contours of constant magnetic field, it is difficult for the H^+ ion to complete a drift through the dayside. If the particle starts closer to the planet on the nightside, its gyro-orbit brings it into contact with the surface of the planet where it will be scattered and lost. Similar to before, an energy of 24 keV is selected since it is the lower energy threshold of the energetic proton sensor [*Andrews et al.*, 2007] on the *MESSENGER* spacecraft and can be used to compare with observations.

[14] The third species traced in Figure 2, and the most abundant heavy ion on Mercury, is Na^+ [*Zurbuchen et al.*, 2008]. These atoms come from the surface of the planet through a number of processes including thermal desorption, photon stimulated desorption, micro-meteoroid vaporization, and solar wind sputtering [*Leblanc and Johnson*, 2003]. The large gyroradius makes it highly nonadiabatic. Through modeling *Yagi et al.* [2010] determined that only Na^+ particles with energies lower than 1 keV could form a trapped population. Na^+ particles that result from solar wind sputtering will be preferentially created near the cusp footprints and over the poles where there are open field lines that allow solar wind plasma to enter. Although Na^+ ions are typically created with energies of a few electronvolts through solar wind sputtering, they quickly gain energies up to hundreds of electronvolts due to centrifugal acceleration while they $\vec{E} \times \vec{B}$ drift from high to low latitudes [*Delcourt et al.*, 2002]. Na^+ particles that gain several keV in energy will not be able to drift around the planet and will be lost quickly as shown in Figures 2e and 2f. The Na^+ is started at $X = -1.2\,R_M$, $Y = Z = 0.0\,R_M$, and a pitch angle of 90°. For comparison, this ion has a gyroradius of 490 km or 0.2 R_M.

4.1. Trapping Geometry

[15] Since energetic electrons can be trapped within Mercury's magnetosphere, a wide range of initial conditions have been tested to study the dynamics of particle drifts. The range of initial conditions for which electrons can be trapped within Mercury's magnetosphere are relatively small in comparison to the Earth. Figure 3 shows results for $\sim 10^4$ electrons with varying start conditions. The X and Y axes are the initial X position and pitch angle, respectively. The color shows the end result of the particle. Start positions are on the nightside ranging from $X_{MSM} = -1.05\,R_M$ to $-1.65\,R_M$ with $Z_{MSM} = Y_{MSM} = 0\,R_M$. The initial energy is constant at $E = 34$ keV, and the pitch angle distribution is isotropic ranging from 0° to 180°. If a particle remained trapped for longer than 80 s (roughly 1.3 drift orbits) in the simulation, it was considered trapped. A particle with an initial pitch angle of 90° can only be trapped if it is within $X \sim -1.25\,R_M$ on the nightside. At larger radial distances, it will drift into the magnetopause and be lost. Due to drift shell splitting, a small number of particles, starting with pitch angles closer to the magnetic field vector but not within the loss cone can remain trapped until near $X \sim -1.65\,R_M$ on the nightside. This is shown by a "forking" of the trapping region around an initial pitch angle of 90°. The energy of each particle is conserved within 0.2% over the drift orbit with our simulation parameters.

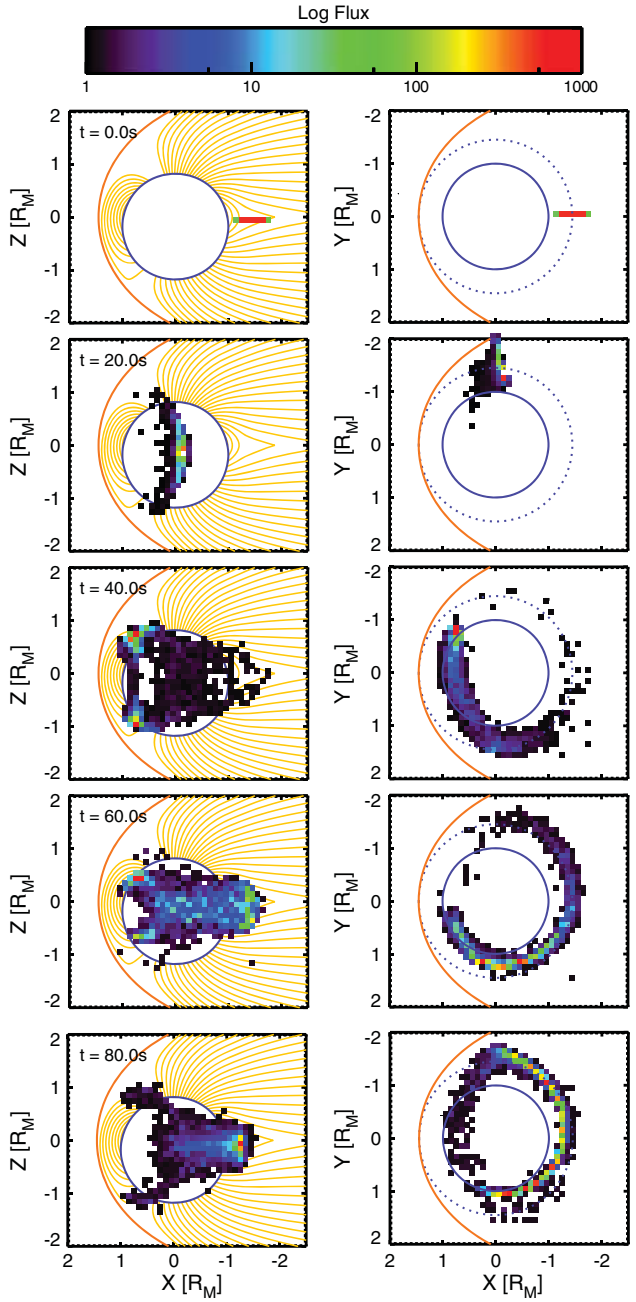

Figure 4. Intensities of 34 keV electrons are shown progressing with time. The left column is an *XZ* cut and the right column is an *XY* cut in MSM coordinates. Each row is a different time step progressing from the first to the fifth row. The dashed line in the right column is the radial distance to the subsolar point on the magnetopause (1.45 R_M). The test electrons are released at start positions on the nightside ranging from X_{MSM} = –1.05 R_M to –1.65 R_M with Z_{MSM} = Y_{MSM} = 0 R_M.

[16] In this simulation, 25% of the particles are lost due to magnetopause shadowing, 54% fall into the loss cone, and 21% remain trapped. The loss cone is largest closest to the planet and is also asymmetric between the north and the south due to the dipole offset. The results show that 2.4 times more particles are lost to the south (light blue) than the north (dark blue). Although we only show that particles can remain trapped for a little over one drift orbit, longer simulations of a steady state magnetosphere at Earth show this orbit can be relatively stable. In tracing many energetic electrons at Earth, *Ukhorskiy et al.* [2011] found an equilibrium state where less than 1% of particles that complete a drift orbit on a bifurcating drift shell are lost over each subsequent drift period.

[17] An additional feature demonstrated in Figure 3 is a distortion of some particles' gyromotion along the magnetopause. When a particle gyrates through the strong magnetic gradients at the magnetopause, the particle can behave nonadiabatically and enter the loss cone. This is shown by the particles lost to the loss cone at the boundary between trapped particles (white) and magnetopause shadowing (red). A contribution to this effect at the boundary may also be from numerical error from the simulation.

[18] The paths of the trace particles in the *XZ* and *XY* planes are shown in Figure 4. All of the electrons that complete a full drift around the planet travel to high latitudes on the dayside due to the compressed magnetic field. The first time step (t = 0 s, first row) shows the start positions near the equator on the nightside. This is similar to the locations of energetic electrons injected from a substorm as suggested from the Mariner 10 observations. As time progresses, the electrons primary gradient and curvature drift toward the dawnside. After 40 s, many of the particles have traveled through the dayside. On the dayside, particles move on bifurcating drift shells to either the northern or southern high latitude. As they drift back to the nightside, they return to the magnetic equator. Since the particles start with different initial pitch angles, they drift at different rates. Particles with pitch angles near 90° will drift the fastest. All of the trapped particles are within a radial distance of 1.5 R_M while on the nightside in the magnetic equatorial plane. In the final time step (t = 80 s, fifth row), electrons have spread out and show the extent of the trapped population. Particles are found at high latitudes on the dayside and are centered on the magnetic equator on the nightside.

5. Discussion

[19] To date, observations by the *MESSENGER* spacecraft provide the best data set to compare with particle simulations. In 2011, *MESSENGER* was inserted into a polar orbit with a periapsis of 200 km above the surface of the planet (1.08 R_M) and apoapsis of 15,000 km (6.15 R_M). The Energetic Particle Spectrometer (EPS) detects energetic electrons and protons with energy ranges of 34 keV to 1 MeV and 25 keV to 2.75 MeV, respectively [*Andrews et al.*, 2007]. *Ho et al.* [2011] summarized the initial findings of the detector showing frequent enhancements of energetic electrons, but no energetic protons. In surveying the electrons, *Ho et al.* [2011] observed enhancements of particles within a radial distance of 1.5 R_M from the planet. On the nightside near midnight, the electrons are observed near the magnetic equator, while on the dayside they are observed off-equator at higher latitudes and sometimes even on open field lines in the cusp [*Ho et al.*, 2012]. In the dawn and dusk sectors, a small enhancement is observed near the equator. These enhancements however are of lower intensity than the ones observed in the noon or midnight sector.

When pitch angle distributions were obtainable within the magnetosphere, they were peaked near 90° [*Ho et al.*, 2012].

[20] In efforts to identify a potential source for the energetic electrons, *Ho et al.* [2012] compared their energy spectra at different locations, finding similar power law slopes at high latitudes on the dayside and near the magnetic equator on the nightside. This led the authors to conclude that a similar source creates both populations.

[21] These observations of energetic electrons and H^+ ions are well described by the model presented in the current study. Our results indicate that the lack of energetic H^+ ions is due to their large gyroradii, which prevent them from completing a drift orbit. If a H^+ ion was energized up to this energy (25 keV), it would spend very little time in the magnetosphere before being lost.

[22] The electron observations are also consistent with the particle tracing in this study. In particular, (1) the electrons are observed near the equator in the midnight sector and at high latitudes on the dayside, (2) the electrons in both regions have a similar power law spectra expected for a single quasi-trapped population, and (3) the electrons are only observed close to the planet typically within a radial distance of 1.5 R_M. Beyond this radial distance, the drift paths lead the electrons into the magnetopause.

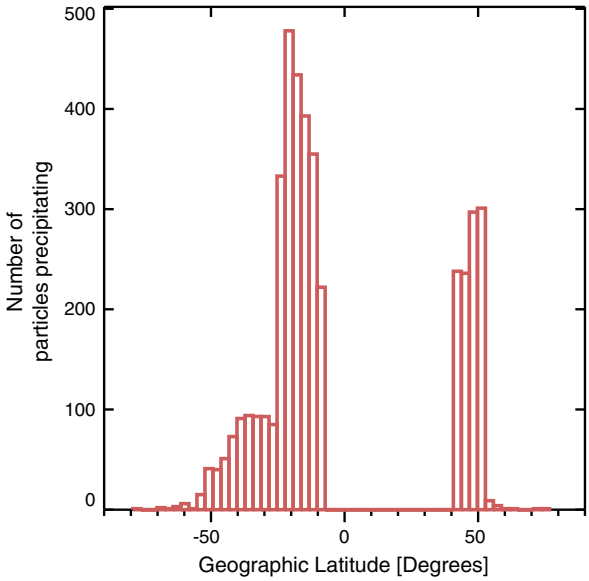

Figure 5. Histogram of the geographic latitudes where charged particles precipitate to the surface of Mercury. The asymmetry is due to the magnetic dipole offset.

5.1. Energetic Particle Sources

[23] Since the trapping region is spatially small and a particle can be lost from the magnetosphere, particularly during times of variable solar wind conditions, one or more active sources are required. Several sources of energization have been suggested thus far and are reviewed below.

[24] From an explanation of the early Mariner 10 observations, it has been proposed that substorms can occur on Mercury [*Siscoe et al.*, 1975]. Recent observations from *MESSENGER* have confirmed the occurrence of substorms [*Sundberg et al.*, 2012]. Through this process, particles on stretched tail field lines can gain energy through betatron acceleration during dipolarization [*Birn and Hesse*, 1994]. Trace particle modeling on Mercury has shown both ions [*Delcourt et al.*, 2010] and electrons [*Delcourt et al.*, 2005] to be energized up to several keV during this process. *Ip* [1997] however modeled H^+ and He^{2+} acceleration up to higher energies (several tens of keV) through dipolarization in Mercury's tail, assuming the process would occur on a time scale of 10 s.

[25] A second source is energization parallel to magnetic field lines due to centrifugal acceleration. Models indicate that this can cause moderate acceleration of cool heavy ions from energies of tens of eV up to hundreds of eV [*Delcourt et al.*, 2002]. As particles near the poles on the nightside $\vec{E}\times\vec{B}$ drift from high to low latitudes, they can be accelerated parallel to the magnetic field line due to a centrifugal force. Because the radius of curvature of the $\vec{E}\times\vec{B}$ drift is much smaller on Mercury than on Earth, this effect is more significant on Mercury. This would populate the midnight sector with high-energy ions.

[26] Finally, it is possible that the energetic electrons are transported from a large planetary magnetosphere with many energetic particles such as Jupiter [*Baker*, 1986]. This source requires magnetic connectivity between Mercury and Jupiter, which may not occur often.

5.2. Quasi-Trapped Particle Precipitation

[27] The atmosphere of Mercury is a tenuous surface-bound exosphere. The most prominent constituents of the exosphere are H, He, O, and Na [*Killen and Ip*, 1999]. Since Mercury lacks an ionosphere or thick atmosphere to absorb collisions with precipitating charged particles, magnetospheric particles in the loss cone collide directly with the surface of the planet. These collisions of magnetospheric particles with the surface can eject surface particles through ion sputtering which contributes to the exosphere. Other exospheric sources include thermal desorption, photon-stimulated desorption, and micro-meteoroid vaporization [*Leblanc and Johnson*, 2003]. Ion sputtering from previously trapped magnetospheric particles will depend greatly on the size of the loss cone or how many charged particles hit the surface. Figure 5 shows the number of precipitating particles with geographic latitude on Mercury from the large-scale electron simulation described earlier. The simulation shows 2.4 times more particles precipitate in the south than in the north as a result of the dipole offset. If sputtering due to the precipitation of electrons is contributing to the exosphere, there should be a north/south asymmetry in the exosphere.

[28] Radiation pressure from the Sun pushes neutral exospheric particles from Mercury in the antisunward direction where they form a tail extending many R_M from the planet [*Baumgardner et al.*, 2008; *Schmidt et al.*, 2012]. The sodium *D* line can be relatively bright and therefore serves as a good probe for exospheric sources. Similar to the asymmetry in the size of the loss cone, ground-based observations from Earth of the sodium tail show two peaks with a north/south asymmetry [*Potter and Killen*, 2008]. The observed asymmetry shows a preference for more particles in the northern tail. Since the combination of radiation pressure and planetary shadowing would send exospheric particles generated in the north to the south and

vice versa, the asymmetric loss cone modeled in this study could explain the asymmetry in the exospheric sodium. The two peaks would also be consistent with exospheric particles being generated preferentially at high latitudes or from precipitating charged particles.

[29] There is also evidence from the first two *MESSENGER* flybys that a majority of the near-planet sodium exosphere forms at high latitudes. Measurements show the sodium emissions peak over the poles and drop off by a factor of 1000 times just $\sim$1 R_M downtail [*Vervack et al.*, 2010]. In contrast to the terrestrial ground-based observations of Mercury, *Vervack et al.* [2010] observed symmetric exospheric sodium emissions from *MESSENGER*. One possible explanation for the potential inconsistency is that the source mechanisms are time dynamic and such an asymmetry is not always present.

6. Conclusion

[30] The drift paths of energetic charged particles are investigated in a modeled magnetic field at Mercury. The drift paths show that a quasi-trapped energetic electron population can exist during steady solar wind conditions; however, energetic H^+ ($E > 24$ keV) and Na^+ ($E > 5$ keV) are unable to complete a full drift orbit due to their large gyroradii. The quasi-trapped energetic electron population drifts through the high latitudes in the dayside magnetosphere and the magnetic equator on the nightside due to the highly compressed magnetosphere. The highly compressed magnetosphere creates a large region within the magnetosphere covering the entire dayside where the minimum magnetic field strength along a field line is found off the equator. Mercury's dipole offset is also significant causing a loss cone that is twice as large in the south than in the north resulting in asymmetric particle precipitation.

[31] **Acknowledgments.** Support was given by the National Science Foundation through grant AGS-1136827. A. S. Ryou and D. G. Sibeck were supported by the THEMIS and RBSP projects. I. I. Alexeev was supported by the Russian Foundation for Basic Research grants 11-05-00894 and 12-02-92600-KO-a, and the European FP7 project IMPEx (262863). The authors would also like to thank A. Glocer, T. Sundberg, and C. Schmidt for useful discussions. Masaki Fujimoto thanks the reviewers for their assistance in evaluating this paper.

References

Alexeev, I. I., E. S. Belenkaya, S. Y. Bobrovnikov, J. A. Slavin, and M. Sarantos (2008), Paraboloid model of Mercury's magnetosphere, *J. Geophys. Res.*, *113*, A12, 12210, doi:10.1029/2008JA013368.

Alexeev, I. I., et al. (2010), Mercury's magnetospheric magnetic field after the first two MESSENGER flybys, *Icarus*, *209*, 2339, doi:10.1016/j.icarus.2010.01.024.

Anderson, B. J., C. L. Johnson, H. Korth, M. E. Purucker, R. M. Winslow, J. A. Slavin, S. C. Solomon, R. L. McNutt Jr., J. M. Raines, and T. H. Zurbuchen (2011), The global magnetic field of Mercury from MESSENGER orbital observations, *Science*, *333*, 1859–1862, doi:10.1126/science.1211001.

Anderson, B. J., C. L. Johnson, H. Korth, R. M. Winslow, J. E. Borovsky, M. E. Purucker, J. A. Slavin, S. C. Solomon, M. T. Zuber, and R. L. McNutt Jr. (2012), Low-degree structure in Mercurys planetary magnetic field, *J. Geophys. Res.*, *117*, E00L12, doi:10.1029/2012JE004159.

Andrews, G. B., et al. (2007), The energetic particle and plasma spectrometer instrument on the MESSENGER spacecraft, *Space Sci. Rev.*, *131*, 523–556, doi:10.1007/s11214-007-9272-5.

Baker, D. N., J. A. Simpson, and J. H. Eraker (1986), A model of impulsive acceleration and transport of energetic particles in Mercury's magnetosphere, *J. Geophys. Res.*, *91* (A8), 8742–8748, doi:10.1029/JA091iA08p08742.

Baker, D. N. (1986), Jovian electron populations in the magnetosphere of Mercury, *Geophys. Res. Lett.*, *13* (8), 789–792, doi:10.1029/GL013i008p00789.

Baumgardner, J., J. Wilson, and M. Mendillo (2008), Imaging the sources and full extent of the sodium tail of the planet Mercury, *Geophys. Res. Lett.*, *35*, L03201, doi:10.1029/2007GL032337.

Belian, R. D., D. N. Baker, E. W. Hones, and P. R. Higbie (1984), High-energy, proton drift echoes: Multiple peak structure, *J. Geophys. Res.*, *89*(A10), 9101–9106, doi:10.1029/JA089iA10p09101.

Birn, J., and M. Hesse (1994), Particle acceleration in the dynamic magnetotail: Orbits in self-consistent three-dimensional MHD fields, *J. Geophys. Res.*, *99*(A1), 109–119, doi:10.1029/93JA02284.

Christon, S. P., S. F. Daly, J. H. Eraker, M. A. Perkins, J. A. Simpson, and A. J. Tuzzolino (1979), Electron, calibration of instrumentation for low energy, high intensity particle measurements at Mercury, *J. Geophys. Res.*, *84*(A8), 4277–4288, doi:10.1029/JA084iA08p04277.

Delcourt, D. C., T. E. Moore, S. Orsini, A. Millilo, and J.-A. Sauvaud (2002), Centrifugal acceleration of ions near Mercury, *Geophys. Res. Lett.*, *29*(12), 1591, doi:10.1029/2001GL013829.

Delcourt, D. C., S. Grimald, F. Leblanc, J.-J. Berthelier, A. Millilo, A. Mura, S. Orsini, and T. E. Moore (2003), A quantitative model of the planetary Na^+ contribution to Mercury's magnetosphere, *Ann. Geophys.*, *21*, 1723–1736, doi:10.5194/angeo-21-1723-2003.

Delcourt, D. C., K. Seki, N. Terada, and Y. Miyoshi (2005), Electron dynamics during substorm dipolarization in Mercury's magnetosphere, *Ann. Geophys.*, *23*, 3389–3398, doi:10.5194/angeo-23-3389-2005.

Delcourt, D. C., T. E. Moore, and M.-C. H. Fok (2010), Ion dynamics during compression of Mercury's magnetosphere, *Ann. Geophys.*, *28*, 1467–1474, doi:10.5194/angeo-28-1467-2010.

Eraker, J. H., and J. A. Simpson (1986), Acceleration of charged particles in Mercury's magnetosphere, *J. Geophys. Res.*, *91*(A9), 9973–9993, doi:10.1029/JA091iA09p09973.

Ho, G. C., et al. (2011), MESSENGER observations of transient bursts of energetic electrons in Mercury's magnetosphere, *Science*, *333*, 1865, doi:10.1126/science.1211141.

Ho, G. C., S. M. Krimigis, R. E. Gold, D. N. Baker, B. J. Anderson, H. Korth, J. A. Slavin, R. L. McNutt Jr., R. M. Winslow, and S. C. Solomon (2012), Spatial distribution and spectral characteristics of energetic electrons in Mercury's magnetosphere, *J. Geophys. Res.*, *117*, A00M04, doi:10.1029/2012JA017983.

Ip, W.-H. (1987), Dynamics of electrons and heavy ions in Mercury's magnetosphere, *Icarus*, *71*, 441–447, doi:10.1016/0019-1035(87)90039-X.

Ip, W.-H. (1997), Time-variable phenomena in the magnetosphere and exosphere of Mercury, *Adv. Space Res.*, *19*, 10, 1615–1620, doi:10.1016/S0273-1177(97)00375-X.

Johnson, C. L., et al. (2012), MESSENGER observations of Mercury's magnetic field structure, *J. Geophys. Res.*, *117*, E00L14, doi:10.1029/2012JE004217.

Killen, R. M., and W.-H. Ip (1999), The surface-bounded atmospheres of Mercury and the Moon, *Rev. Geophys.*, *37* (3), 361–406, doi:10.1029/1999RG900001.

Leblanc, F., and R. E. Johnson (2003), Mercurys sodium exosphere, *Icarus*, *164*, 261–281, doi:10.1016/S0019-1035(03)00147-7.

Ness, N. F., K. W. Behannon, R. P. Lepping, Y. C. Whang, and K. H. Schatten (1974), Magnetic field observations near Mercury: Preliminary results from Mariner 10, *Science*, *185* (4146), 151–160, doi:10.1126/science.185.4146.151.

Öztürk, M. K., and R. A. Wolf (2007), Bifurcation of drift shells near the dayside magnetopause, *J. Geophys. Res.*, *112*, A07207, doi:10.1029/2006JA012102.

Potter, A. E., and R. M. Killen (2008), Observations of the sodium tail of Mercury, *Icarus*, *194*, 1–12, doi:10.1016/j.icarus.2007.09.023.

Schmidt, C. A., J. Baumgardner, M. Mendillo, and J. K. Wilson (2012), Escape rates and variability constraints for high-energy sodium sources at Mercury, *J. Geophys. Res.*, *117*, A03301, doi:10.1029/2011JA017217.

Schriver, D., et al. (2011), Quasi-trapped ion and electron populations at Mercury, *Geophys. Res. Lett.*, *38*, L23103, 23103, doi:10.1029/2011GL049629.

Shabansky, V. P. (1971), Some processes in the magnetosphere, *Space Sci. Rev.*, *12*(3), 299–418, doi:10.1007/BF00165511.

Siscoe, G. L., N. F. Ness, and C. M. Yeates (1975), Substorms on, Mercury? *J. Geophys. Res.*, *80*(31), 4359–4363, doi:10.1029/JA080i031p04359.

Slavin, J. A., et al. (2009), MESSENGER observations of magnetic reconnection in Mercury's magnetosphere, *Science*, *324*, 606–610, doi:10.1126/science.1172011.

Slavin, J. A., et al. (2010), MESSENGER observations of extreme loading and unloading of Mercury's magnetic tail, *Science*, *329*, 665–668, doi:10.1126/science.1188067.

Sundberg, T., et al. (2012), MESSENGER observations of depolarization events in Mercurys magnetotail, *J. Geophys. Res.*, *117*, A00M03, doi:10.1029/2012JA017756.

Trávníček, P. M., P. Hellinger, and D. Schriver (2007), Structure of Mercury's magnetosphere for different pressure of the solar wind: Three-dimensional hybrid simulations, *Geophys. Res. Lett.*, *34*, L05104, doi:10.1029/2006GL028518.

Trávníček, P. M., P. Hellinger, D. Schriver, D. Herčík, J. A. Slavin, and B. J. Anderson (2009), Kinetic instabilities in Mercury's magnetosphere: Three-dimensional simulation results, *Geophys. Res. Lett.*, *36*, L07104, doi:10.1029/2008GL036630.

Ukhorskiy, A. Y., M. I. Sitnov, R. M. Millan, and B. T. Kress (2011), The role of drift orbit bifurcations in energization and loss of electrons in the outer radiation belt, *J. Geophys. Res.*, *116*, A09208, doi:10.1029/2011JA016623.

Yagi, M., K. Seki, Y. Matsumoto, D. C. Delcourt, and F. Leblanc (2010), Formation of a sodium ring in Mercury's magnetosphere, *J. Geophys. Res.*, *115*, A10253, doi:10.1029/2009JA015226.

Vervack, R. J., Jr., W. E. McClintock, R. M. Killeen, A. L. Sprague, B. J. Anderson, M. H. Burger, E. T. Bradley, N. Mouawad, S. C. Solomon, and N. R. Izenberg (2010), Mercury's complex exosphere: Results from MESSENGER's third flyby, *Science*, *329*, 672–675, doi:10.1126/science.1188572.

Wan, Y., S. Sazykin, R. A. Wolf, and M. K. Öztürk (2010), Drift shell bifurcation near the dayside magnetopause in realistic magnetospheric magnetic fields, *J. Geophys. Res.*, *115*, A10205, doi:10.1029/2010JA015395.

Zurbuchen, T. H., J. M. Raines, G. Gloeckler, S. M. Krimigis, J. A. Slavin, P. L. Koehn, R. M. Killen, A. L. Sprague, R. L. McNutt Jr., and S. C. Solomon (2008), MESSENGER observations of the composition of Mercury's ionized exosphere and plasma environment, *Science*, *321*, 90–92, doi:10.1126/science.1159314.